Bulletin of Earthquake Engineering (2021) 19:2867–2891
https://doi.org/10.1007/s10518-021-01089-x

ORIGINAL ARTICLE

Innovative technique to develop fragility curve based on state-based philosophy

Aref Baharvand[1] · Abdolrasoul Ranjbaran[2] · Mohammad Baharvand[3]

Received: 22 June 2020 / Accepted: 29 March 2021 / Published online: 16 April 2021

Abstract

The fragility curves are known as an efficient probabilistic-base tool used to evaluate vulnerabilities in various fields. However, accurate access to these curves has always been associated with complexities that have made it difficult for structural designers to achieve. Many attempts have been made to provide a new fragility function using State-based philosophy (SBP) theory to replace the conventional fragility function in recent years. A method in which gradual changes in structural properties due to a destructive factor is generally used to ultimately create a function with a new structure to describe the structure's fragility. In this study, after the usual method of obtaining the fragility curve is briefly reviewed, the new structure proposed for the fragility function by SBP will be explained. A completely new technique will then be introduced using a combination of selected (and not complete) information from the usual incremental dynamic analysis method in the SBP fragility function. The result is a fragility curve with perfectly acceptable accuracy that computational efforts to achieve have been dramatically reduced. This claim's validity is examined by performing this technique on some two-dimensional special moment frames models, and its advantages and disadvantages and accuracy are further explored.

Keywords Probabilistic seismic demand models · Performance-based earthquake engineering · State-based philosophy · Fragility curve · Fragility function · Incremental dynamic analysis

Abbreviations

CDF Cumulative distribution function
CP Collapse prevention

✉ Aref Baharvand
ar.baharvand@shirazu.ac.ir

Abdolrasoul Ranjbaran
aranjbaran@yahoo.com

Mohammad Baharvand
Baharvand12@gmail.com

[1] Department of Civil and Environmental Engineering, Shiraz University, 8179976474 Esfahan, Iran

[2] Department of Civil and Environmental Engineering, Shiraz University, Shiraz, Iran

[3] Department of Architecture, Faculty of Engineering and Architecture, Istanbul Gelisim University, Istanbul, Turkey

EDP	Engineering demand parameter
Err	Error
IDA	Incremental dynamic analysis
IO	Immediate occupancy
IM	Intensity measure
LS	Life safety
NC	Not considered
MSA	Multiple-stripe analysis
NSA	Nonlinear static analysis
PBEE	Performance-based earthquake engineering
PDF	Probability distribution function
PEER	Pacific earthquake engineering research
PGA	Peak ground acceleration
PSDM	Probabilistic seismic demand models
PSDA	Probabilistic seismic demand analysis
RSA	Response spectrum analysis
RTR	Record-to-record
SBP	State-based philosophy
SD	Standard deviation
SDOF	Single degree Of freedom
SMF	Special steel moment frame
St	Story
THA	Time-history analysis

1 Introduction

Earthquakes are known as one of the most destructive natural disasters that inflicted many casualties on human society. In urban areas, what really causes an earthquake to have such fatal consequences is the comparative lack of accurate seismic risk prediction in structures' design procedure. Therefore, to overcome the problem of non-safety in diverse structure systems, many researchers have focused their studies on the improvement of some methods that can predict the vulnerability of structures to future earthquakes. Gradually, the results of these studies were reflected in seismic codes. Hence, in the last two decades, dramatic changes are seen in the way seismic codes encounter this challenge (Vargas et al. 2013; Kappos 2016; Hasik et al. 2018; Cremen and Baker 2018).

Nowadays, one of the most popular tools for the probabilistic safety assessment of structures is fragility analysis, so it has become a topic of interest among researchers in recent decades. In fact, fragility analysis can predict an engineered structure system or even a structural member's ability to resist against a special destructive phenomenon such as a devastating earthquake or flood (B. Tekie and R. Ellingwood 2003; Jalayer et al. 2014; Michel et al. 2018; Bakalis and Vamvatsikos 2018).

Generally, a seismic fragility analysis of a structure is summarized within a definition of a fragility function, and its *illustration known as "fragility curve*". To be more specific, what is being studied in a particular fragility analysis is a relative comprehension of comparison between the seismic capacity and the seismic demand of the intended structure system (E. Padgett and DesRoches 2008). The fragility analysis of a structure can finally result in a conditional probability of a seismic demand (D) which exceeds the pre-determined

structural performance level as a term of a seismic capacity (C) in a pre-decided level of ground motion intensity measure (IM). This way for the description of the seismic fragility function is expressed in Eq. (1):

$$P(Fragility) = P[C \leq D|IM] \tag{1}$$

To express seismic demand, which is appropriate to use in Eq. (1), coordinated probabilistic seismic models should be developed. The fragility function can be obtained by combining the seismic structure models' responses and structural performance levels. Finally, this function can be considered a probabilistic criterion for assessing new or pre-existing structural systems or members' seismic resistance.

So far, various strategies have been applied to estimate proper fragility function. These strategies differ in many aspects, such as using different approaches to obtain seismic damage data. To be exact, the judgmental approach, field observations of damage after earthquakes, static structural analyses, and finally, dynamic analytical simulation are known as the most important strategies to estimate damage data (Shafei et al. 2011; Baker 2015). Dynamic analytical simulation is used widely in recent research since it offers the investigator the capability to control collected damage data. Another important issue that needs to be addressed before conducting the analyses is deciding on the IM levels and the number of analyzes performed at each IM level. The fragility function obtained through this way is typically called the analytical fragility function (E. Padgett and DesRoches 2008; Casotto et al. 2015; Noh et al. 2015; Xin et al. 2018).

To date, numerous procedures have been proposed for conducting nonlinear dynamical analyses to provide appropriate damage data as a result. One of the most widely used methods is known as Incremental Dynamic Analysis (IDA). In this method, a proper selective group of ground motions is frequently scaled until the structure reaches its collapse level under excitation caused by each of them (Vamvatsikos and Cornell 2002, 2004; FEMA 2009).

A challenging matter raised by the utilization of IDA analysis was selecting appropriate IM levels. The step-by-step algorithm in which IM levels increase with a constant rate from zero to its corresponding collapse value has been known as the simplest solution for this problem (Yun et al. 2002). Although this algorithm is simply programmable, it suffers from two major drawbacks. First, it is not so cost-effective, and second, the quality of this algorithm largely depends on the value of the incremental step of IM. Therefore, researchers tried to apply appropriate advanced record scaling algorithms, resulting in significantly reducing computational costs. The technique that solved these problems is known as the "*hunt & fill*" process in which a small amount of IM was used as an initial level for seismic analysis. Next, the hunt phase begins with a consecutive increase in step value until reaching the collapse level. Finally, in the Fill phase, the additional analysis levels are considered at intervals of the hunt phase points to increase the accuracy. A newer approach which is presented to obtain the fragility curve is the so-called "*multiple-stripes*". In fact, this method was presented so that dissimilar groups of seismic records are selected and applied to the structural model for a specified IM level (Jalayer 2003).

Although researchers have proposed several methods to obtain fragility function, this study offers a totally new and innovative strategy to tackle the problem of time-consuming and innumerable computational efforts to obtain a fragility curve. The theory of State-Based Philosophy (SBP), which was first introduced by Ranjbaran, will be applied to achieve this goal (Ranjbaran et al. 2016). Based on extensive investigations regarding the behavior of natural phenomena, the state-based-philosophy is detected and developed.

Making use of logical reasoning and concise mathematics, the basic formulation for the proposed method is derived. The outcome of the work is expressed as a function of functions called the Persian Curve. The Persian Curve is a function of the state functions and two control parameters. State functions are explicit functions of the state variable. The state variable is defined in a unit interval with a zero value at the origin and a unit value at the destination. The control parameters are obtained from the calibration of the reliable data as follows. The proposed method applies to all natural phenomena that are considered the change in the system's state.

In fact, this theory has many applications and different branches. One of its products is the SBP fragility function, which can act as an appropriate alternative for current fragility functions. The ability and capability of SBP theory in drawing fragility curves is a topic that has recently been considered and confirmed (Baharvand and Ranjbaran 2020a, b). The SBP fragility function's unique capability enables it to considerably reduce the number of nonlinear time-history analyses without significantly reducing the accuracy of fitting the fragility curve process. This issue will be further explored by conducting a case study investigation. Finally, the SBP fragility function will be present as a more efficient attitude to draw fragility curves, and its advantages and drawbacks will be discussed.

2 Conventional analysis strategies to obtain fragility curve

In the literature of performance-based earthquake engineering (PBEE) framework, the parameter used to describe the intensity of the earthquake is called Intensity Measure (IM, e.g., first mode acceleration), and structural responses are also indicated by one or more Engineer Demand Parameter (EDPs, e.g., maximum inter-story drift ratio). Moreover, the relations that can describe the dependency between IM and EDP are called Probabilistic Seismic Demand Models (PSDMs).

To achieve proper PSDMs, at the first step, it is necessary to evaluate the response of the structures under different ground excitations by performing Probabilistic Seismic Demand Analysis (PSDAs). So far, many different methods have been used to conduct PSDA. These methods vary in different ways, including restrictive requirements in the analysis process, predicting structural responses, computational effort, and results' accuracy. There are almost three major categories of PSDAs. First, methods based on a series of the Time-History Analysis (THA), second, those based on Nonlinear Static Analysis (NSA), and third, methods based on Response Spectrum Analysis (RSA). Among these categories, time-history analysis benefits from significant advantages over two other groups. Two major reasons bring about this excellence. First, these types of analysis can consider the input ground motions' fundamental characteristics during the analysis. Second, they can consider both nonlinear behavior sources (material and geometrical nonlinearities) in the numerical model with relatively higher accuracy. Nevertheless, some of the THA methods are more popular and widely used in PBEE framework. Incremental Dynamic Analysis (IDA), cloud analysis, and Multiple-Stripe Analysis (MSA) are known as the most efficient techniques among all THA methods.

IDA procedure is selected to achieve the purpose of this. This method can be considered a dynamic equivalent of the familiar static pushover analysis since there are fundamental similarities between these two analyses. In the first step of IDA, a set of ground motion records with appropriate characteristics must be selected. Recognition of these records' suitability is possible by considering the regional seismic hazard and the desired

performance limits states. However, standard protocols have also been developed to cover almost all types of ground motion records to ensure that the Record-To-Record (RTR) variability is taken into account with proper precision. Therefore, additional unnecessary efforts for selecting suitable ground motions are avoided. One of these standard protocols presented in FEMA P-695 document that 22 pairs of far-field ground motions (44 single ground motions) are introduced and used in this study (ATC 2009).

After ground motion selection, the next step includes determining the class of structure and proper EDP. This EDP should be measured to evaluate the structural response to the input ground motion during the analysis process. Developing a detailed finite element model for an intended class of structure seems necessary to capture selected EDP values during the THA. Next, all of the selected records need to be scaled by using the same IM. Various definitions have been recommended appropriate for the IM by researchers, but the most widely used IM for building structures has been the spectral acceleration at the fundamental period T_1, which is characterized by $S_a\left(T_1,\zeta\right)$. Then, the intensity of these scaled records continuously grows by using increasingly coefficients. The next step is applying them to the structure to perform a nonlinear THA and attain EDP's extreme values for each analysis. This process continues until all pre-determined performance levels are achieved. The last step is developing an appropriate demand model between resulting EDPs and predetermined IMs to obtain fragility function. Of course, there are several ways to do this step.

As mentioned before, a fragility function of a structure can be considered a probabilistic function regarding IM. To make this issue more clear, it is useful to return to Eq. (1). This equation gives the probability of exceeding a limit state at the given level of IM as an output. In PBEE literature, two different approaches have been used to define seismic demand D and seismic capacity C: EDP-based approach and IM-based approach. In previous researches, the IM-based approach has been used to achieve the collapse fragility curve in which structure experiences dynamic instability. In this technique, IMs are directly used to estimate the probability of collapse of the building. The IM corresponds to this particular structural damage level is called'collapse capacity' and is denotes as IM_c. In the IM-based approach, demand and capacity are characterized by their IM counterparts. As a result, fragility curves describe the probability of collapse given the value of IM, as shown in Eq. (2):

$$P\left[C|IM=im_i\right]=P[IM_c<IM=im_i] \tag{2}$$

After obtaining the values of IM_c for each ground motion obtained from IDA analysis, appropriate statistical parameters such as median and standard deviation of the $\ln(IM_c)$ can be obtained simply. So, the plot of the obtained log-normal Cumulative Distribution Function (CDF) represents the collapse fragility curve.

On the other hand, in the EDP-based approach, both seismic demand and seismic capacity are defined in terms of EDP and characterized by EDP_d and EDP_c, respectively. These parameters are potentially random quantities estimated in a probabilistic manner. Therefore the probability of limit state exceedance can be defined as Eq. (3) (Zareian et al. 2010):

$$\begin{aligned} P[D\geq C|IM] =& P\left[EDP_d\geq EDP_c|IM=im_i\right] \\ =& \sum_{allepd_c} P\left[EDP_d\geq EDP_c|EDP_c=edp_c,IM=im_i\right]P\left[EDP_c=edp_c\right] \end{aligned} \tag{3}$$

In Eq. (3), the term $P\left[EDP_d \geq EDP_c | EDP_c = edp_c, IM = im_i\right]$ represents the probability that the demand exceeds the capacity quantity $EDPc$ at given $IM = im_i$, and the term $P\left[EDP_c = edp_c\right]$ illustrates the probability that the capacity is equal to $EDPc$. Despite Eq. (3) 's slightly complex appearance, this equation is widely used to determine the fragility function. In this study, the EDP-based approach using deterministic EDP_c is used to achieve the fragility curves. In this case, term $P\left[EDP_c = edp_c\right]$ in Eq. (3) will be equal to one.

3 SBP fragility functions

Stiffness or flexibility of any structure can be considered as one of its inherent features. In other words, in any structure (with any size or application and made with any materials), these two properties will be recognizable, and they can be expressed quantitatively. Of course, these two properties can also be considered as a single property because the value of one of them is equal to the inverse of the other. If a structure's stiffness and flexibility are symbolized with k_S and f_S, respectively, this inverse relationship can be shown as $f_S = 1/k_S$. In the SBP procedure, unlike the process used in finite elements, there is no need to extract these two parameters in their exact form. Stiffness and flexibility can build the foundation of formulating the phenomenon functions, as will be mentioned later.

The reason that causes the reduction of structural stiffness and increment of structural flexibility is called the'*damage source*' . According to its type, a wide range of phenomena can be known as the damage source for a determined structure. For example, this damage source can be considered an earthquake, fire, or even an explosion for a steel building structure. However, no matter the cause of the damage to the structure, there will be a common occurrence in all of them, which is the starting of reducing stiffness and increasing the flexibility procedure of the structure immediately after the structure's damage begins.

If the damage source provides sufficient intensity, this process will continue until the structure collapses. Therefore, the stiffness of a structure that was considered k_S in an intact state decreases steadily. As a result, the stiffness value will be zero when the structure reaches its collapse limit state. During this path, the reduced stiffness of the structure (k_{DS}) will be equal to the stiffness of the intact structure (k_S) minus the lost stiffness due to the damage source (k_D). This relationship between various stiffnesses is shown in Eq. (4):

$$k_{DS} = k_S - k_D \tag{4}$$

On the other hand, the flexibility of the intact structure (f_S) increases continuously due to the damage that occurs to the structure. The flexibility ultimately becomes infinite when the state of the structure is so close to collapse. In the case where the structure is between the intact and the complete collapse states, its flexibility can be expressed as Eq. 5:

$$f_{DS} = f_S + f_c \tag{5}$$

In Eq. 5, f_{DS} denotes the flexibility of the damaged structure, and f_c is the flexibility magnitude which decreased from the flexibility of the intact structure because of the damage source. The fundamental relationship between the stiffness and the flexibility of a structure implies that the result of their multiplication in each case (intact or damaged) should be equal to one. If this relation is applied to the stiffness and the flexibility of the damaged structure given in Eq. (4) and Eq. (5) respectively, Eq. (6) will be obtained:

$$\left(k_S - k_D\right)\left(f_S + f_c\right) = 1 \tag{6}$$

If Eq. (6) is solved for the lost stiffness due to the damage source (k_D), Eq. (7) will be obtained:

$$k_D = F_R k_S F_R = f_c / \left(f_s + f_c\right) \tag{7}$$

In Eq. (7), F_R is a function that represents the amount of structural damage progress. Before the damage begins, its value is zero, and as the structure begins to damage its magnitude increases steadily until the ultimate collapse state. At this point, the value of the F_R function will be equal to one. It is obvious that ($F_R = 0$) is minimum value for ($f_c = 0$) and ($F_R = 1$) is maximum value for ($f_c = \infty$). Consequently, the derivative of F_R at two ends are zero. In SBP, it is assumed that F_R function can play the role of fragility function of the structure when it has the following three properties simultaneously. The first is that this function must be continuous. The second is that F_R should have derivative, and the third is that the values of the first derivative of the F_R at both ends of its domain must be zero. Like the other functions introduced in SBP, this function's domain is the interval between the minimum and maximum intensity measure of the earthquake ($Z \in \left[IM_{min}, IM_{max}\right]$). Its domain is an interval between zero and one ($\xi \in [0,1]$) in the standardized form.

As a result, if a suitable formulation can be found for the F_R function that satisfies all the above-mentioned constraints, it can be used as a fragility function. Such a formulation has previously been proposed in SBP (Ranjbaran and Ranjbaran 2016). Hence, the function F_R is called the' *SBP fragility function*'. The final structure of the SBP fragility function is achievable in Eq. (8):

$$F_R(\xi) = \frac{(k_N^2 D(\xi))^p}{O(\xi)^q + (k_N^2 D(\xi))^p} \tag{8}$$

There are two functions and three constant parameters in Eq. (8). Two functions used in this equation are' D' and' O', which are called' *destination function*' and' *origin function*', respectively. Three constant parameters in Eq. (8) are k_N, p and q. The first parameter (k_N) is called' *natural failure criterion*' and the second and third parameters (p and q) are power factors associated with the destination and origin functions, respectively. In destination and origin functions, only one independent variable has been used, which called' *state variable*' and characterized by' ξ'. A state variable is a standardized variable that can only accept values between zero and one. Therefore, to prepare inputs for the destination and origin functions by using N data from random variable Z, it is first necessary that these data be normalized between zero and one. This normalization performs through Eq. (9):

$$\xi_i = \frac{Z_i - \min\left(Z_i\right)}{\max\left(Z_i\right) - \min\left(Z_i\right)} \quad 1 \le i \le N \tag{9}$$

Destination and origin functions, which are defined in SBP, the same as the F_R function, must have three important properties: continuity, differentiability, and zero first-order derivatives at both ends of the domain. Here, the domain is exactly the range described for the F_R function. Also, in destination, the function's values must be equal to zero and one at the beginning and end of the domain, respectively. The origin function values at the beginning and end of its domain must also be equal to one and zero, respectively. Note again that the domain definition is the same for all functions used in SBP.

The best and simplest formulation for these functions can be obtained from combining polynomial and trigonometric expressions by applying this technique, two examples purposed in Eqs. (10a) and (10b) for origin and destination functions.

$$O(\xi) = 0.25\left(3 - 6\xi^2 + 4\xi^3 + cos(\pi\xi)\right) \tag{10a}$$

$$D(\xi) = 0.25\left(1 + 6\xi^2 - 4\xi^3 - cos(\pi\xi)\right) \tag{10b}$$

By re-examining the structure of the fragility function introduced in Eq. (8) and according to what was obtained in Eq. (8) for the origin and destination functions (O and D), it is determined that two types of input data are required to form the SBP fragility function. The first input is the values of the O and D functions for different IM values, and the second required data is the values of three constant parameters (k_N, p and q).

4 Model properties

To verify the technique to achieve the fragility curve introduced in this study, it is necessary to implement this technique on numerical models and examine its results. These numerical models were selected from the type of two-dimensional special steel moment frame (SMF) and a plan, as shown in Fig. 1a, was considered for these frames. Due to the plan's symmetry and the perimeter lateral load resisting system, this plan's analyzing results can be obtained by modeling the selected two-dimensional frame with appropriate approximation. (Fig. 1b). Four 2D SMF frames (2-St, 4-St, 8-St, and 12-St) were modeled and used for fragility analysis in this study.

In the following, some important details of these frames, which are effective in their seismic behavior, will be described. The amount of dead loads and live loads that have not been reduced are 4.5 kN/m2 and 2.5 kN/m2, respectively. These loads were considered uniformly on the surface of all stories. Urban California was selected as the assumptive site to construct these models which has a high seismic hazard (SDC = Dmax) and soil of class D. In the design process, 0.04 radians was considered as a limit for inter-story drift angels of beam to column connections. It is assumed that all the columns and beams in these models are made of ASTM A992 Gr. 50 steel with 345 MPa nominal yield strength.

The framework of the open-source software OpenSees (Mazzoni et al. 2006) was chosen for the modeling process. To model SMF frames, several modeling methods are provided by OpenSees. To achieve the goals considered in this study, SMF models should be created by an inelastic analysis approach. The inelastic approach itself can be used in two ways: models with distributed inelasticity or models that benefit from lumped or concentrated inelasticity. What differentiates these approaches is how plasticity is distributed in structural elements. The second method mentioned above was selected for modeling in this study. Thus, all the inelastic behaviors of the structural members were concentrated in certain parts that can become a plastic hinge (Fig. 1c). In these places, some lumped springs are placed virtually, and in the next step, a special behavior is defined for these springs. Such a definition is based on parameters that researchers have already obtained and can accurately predict member behavior in the nonlinear range.

The defining parameters of the structural members' nonlinear behavior actually indicate a moment–curvature diagram confirmed in practical experiments. An important point to consider in defining the moment–curvature curve is to consider cyclic deterioration

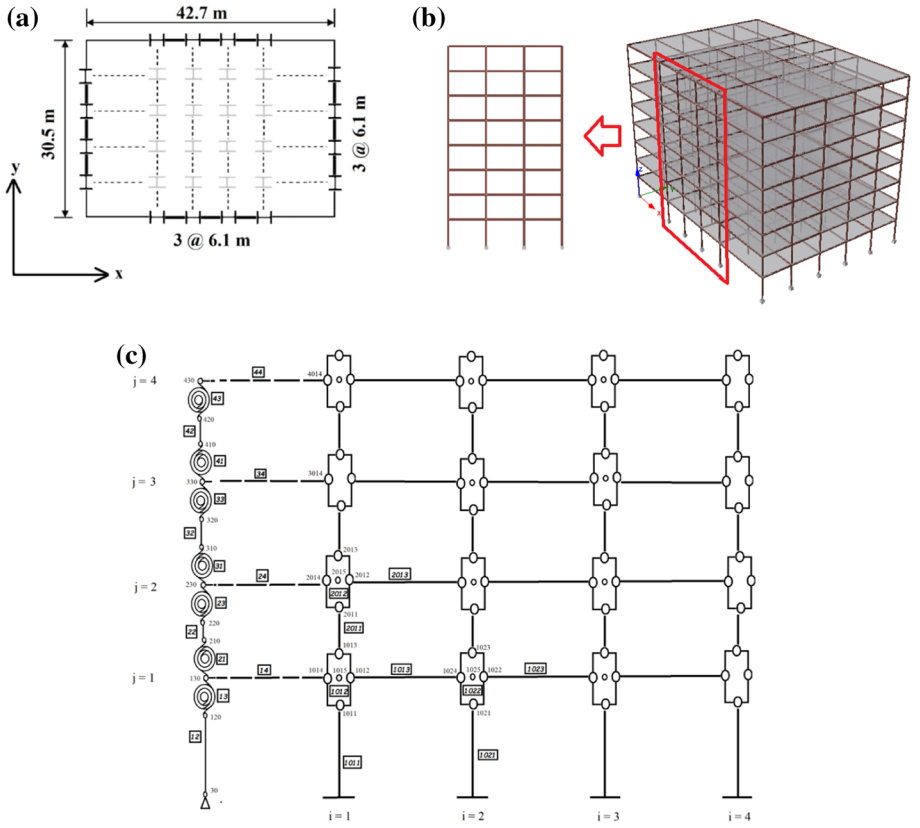

Fig. 1 **a** The plan of the SMF building, **b** Selected 2D frame in an 8-story SMF building, **c** Schematic view of SMF frame modeled in OpenSees

phenomenon. Regression relations mainly express these parameters. For beam elements, Elkady and Lignos (Elkady and Lignos 2014) and Lignos et al. (Lignos and Krawinkler 2011) proposed relationships that were used in many previous studies and are used in this study as well. Similarly, Hartlope and Lignos suggested such relationships for column members, used in column modeling in this study. (Hartloper and Lignos 2017).

Since these models are the same as the models used in the previous two studies, further explanations are avoided for brevity. Refer to References (Baharvand and Ranjbaran 2020a) and (Baharvand and Ranjbaran 2020b) for more details on the models.

5 Maximum IMs determination

For the purposes of PBEE different forms and numbers of IM are used to describe characteristics of each ground motion of interest. The variation in IM selection is due to the different types of structures and information that can be accessed from each IM. For the buildings that dominant modes of vibration are the first mode, displacements do not enter the nonlinear region. Therefore, a standard choice for IM can be the first mode (pseudo)

spectral acceleration in the specific damping, which is characterized by $\mathrm{Sa}(T_1, \zeta)$ (Shome and Cornell 1999; Vamvatsikos and Cornell 2005). In this research, due to the type of building structure modeled (special steel moment frame),$\mathrm{Sa}(T_1, \zeta = 2\%)$ is used as IM.

Determining the maximum IMs ($=\mathrm{Sa}(T_1, \zeta)$) for each EDP capacity limit state (e.g., IO, LS, and CP) among all ground motion of interest is one of the key stages for specifying of SBP fragility function. The importance of determining these IM values is that in the process of normalizing the data in Eq. (9) term "$\max(Z_i)$" will be replaced by these parameters. For more brevity, maximum IMs for different $\mathrm{EDP_c}$ are symbolized by $\mathrm{Sa}^{\mathrm{IO}}_{\mathrm{max}}$,$\mathrm{Sa}^{\mathrm{LS}}_{\mathrm{max}}$, and $\mathrm{Sa}^{\mathrm{CP}}_{\mathrm{max}}$ for immediate occupancy, life safety, and collapse prevention target building performance levels, respectively.

With a closer look at the IDA (or MSA) analysis results, it can be concluded that after passing the region of elastic behavior, maximum IMs were obtained by individual IDA curves associated with one or two specific ground motion records. Thus, if somehow such a ground motion record can be found by performing IDA analyses for that particular record and without the requirement of performing IDA analyses for other records, the maximum IM parameters for all EDP capacity limit states can be obtained. In this study, a record with such a feature is called'*extreme record*'. Although this assumption is generally correct, it may be violated in some limited points under certain circumstances. It should be noted that these points will not form a significant range of structural behavior. Even in this case, although the method's accuracy will be slightly lower, the results will still be acceptable. In other words, a ground motion record that is thought to produce maximum IMs in all EDPs only produces maximum responses in the majority regions of EDP. In some limited regions, other records produce these extreme parameters. Figure 2 shows a good example of this situation in some limited EDP regions. As a result, a discussion about the degree of accuracy and a comparison between this assumption's advantages and disadvantages can be made after modeling and finding related SBP fragility functions.

However, the challenge that must be solved at this stage is how to find the extreme record and how to minimize the effort to find it. To find such a solution, it is enough to note a simple relationship between IMs and EDPs. Normally in an IDA analysis, the ground motion record that needs the largest IM for producing the constant EDP is the same ground motion that produces the lowest EDP in a constant IM structure. In fact, this is another expression of the ascending trend of each IDA curve, which is true as general behavior. However, it is also violated in some limited points. Therefore, it can be concluded that the appropriate solution for finding extreme records is an IDA analysis in a single selective strip of IM (pseudo single strip analysis). Since completing the necessary analytical data to fit the fragility curve on them, needs performing similar pseudo-multiple-strips analysis and also the IM used in this study is a type of first mode spectral acceleration, the IM strip used to determine extreme record is symbolized by S_a^{Int} (Fig. 2). Note that superscript' *Int* ' refers to the word "Initial" because the S_a^{Int} represents the initial strip value for structural analysis.

Another important issue for selecting S_a^{Int} is that the selected value must be restricted to a certain range. This value should not be selected so small that it is placed in the region of the structure's linear-elastic behavior. In this region, the difference between EDPs is much smaller, leading to the correct selection of extreme records. On the other hand, if the value of S_a^{Int} is chosen very large, all ground motion records in that IM scale may cause a global collapse in the structure, and as a result, there will be no data to determine the extreme record. For the SMF structure system investigated in this study, the range between $1\mathrm{g} \le \mathrm{S_a^{Int}} \le 4\mathrm{g}$ was appropriate.

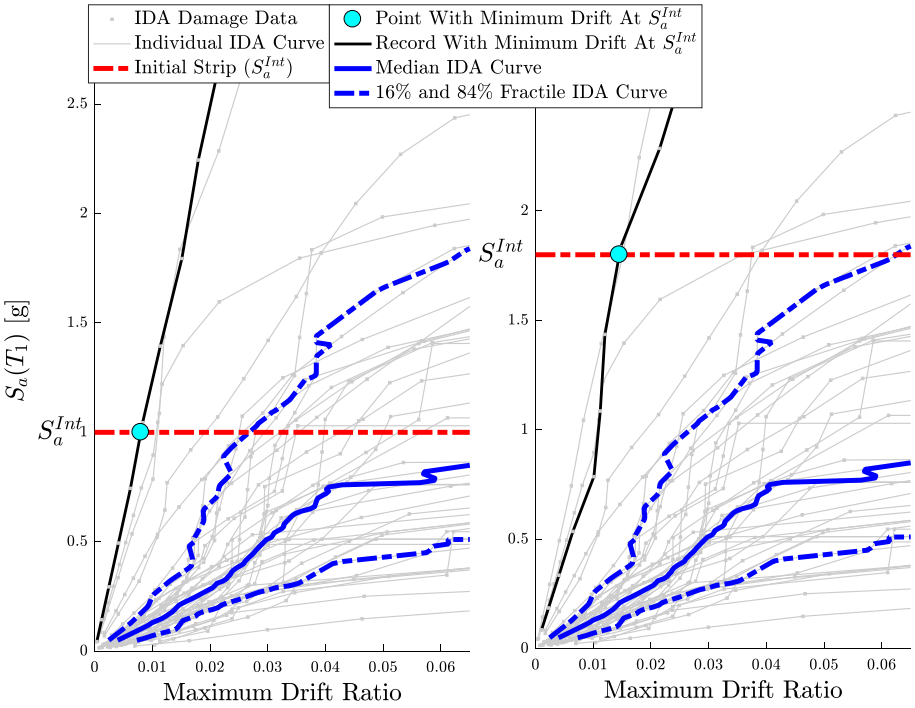

Fig. 2 Various choices for S_a^{Int} for an 8-story SMF frame have led to select different ground motion records as the extreme record

After identifying the extreme record, the IDA analyses using this record can be performed until the response of structure riches the largest EDP capacity limit state. Thus, the maximum IMs related to each EDP capacity (here, target building performance levels) are obtained by IDA analyses using only one ground motion record. By using this simple technique, the goal of determining the term "$\max(Z_i)$" in Eq. (9) will be achieved with the least possible effort. Figure 3 illustrates an example of using this technique.

The essential comment about the difference between multiple-strip analysis and the IDA analysis's special application applied in this study (called pseudo-multiple-strip analysis) should be present here. In Fig. 4, several IM strips, including S_a^{Int} and some other strips in case of using pseudo-multiple-strip analysis, are determined as an example to clear the subject. In this figure, the blank circles on each IM strip show the response of a structure under excitation of those ground motion records which were unable to create such a strong EDP response that can satisfy the intended EDP capacity level (here collapse limit sate). Additionally, numbers inserted to the left column represent the number of records that could satisfy that EDP capacity level at that certain IM strip.

Such a configuration of analyses is partially similar to multiple-strips analyses in the earthquake engineering literature. Therefore, the multiple-strip analysis can be considered a special type of IDA analysis with some differences from the original method. In this type of analysis, several IM levels are selected, and EDP data are also obtained by performing nonlinear time history analysis using ground motion records specified for each IM level before [10]. The process of selecting appropriate ground motion records in each IM stripe

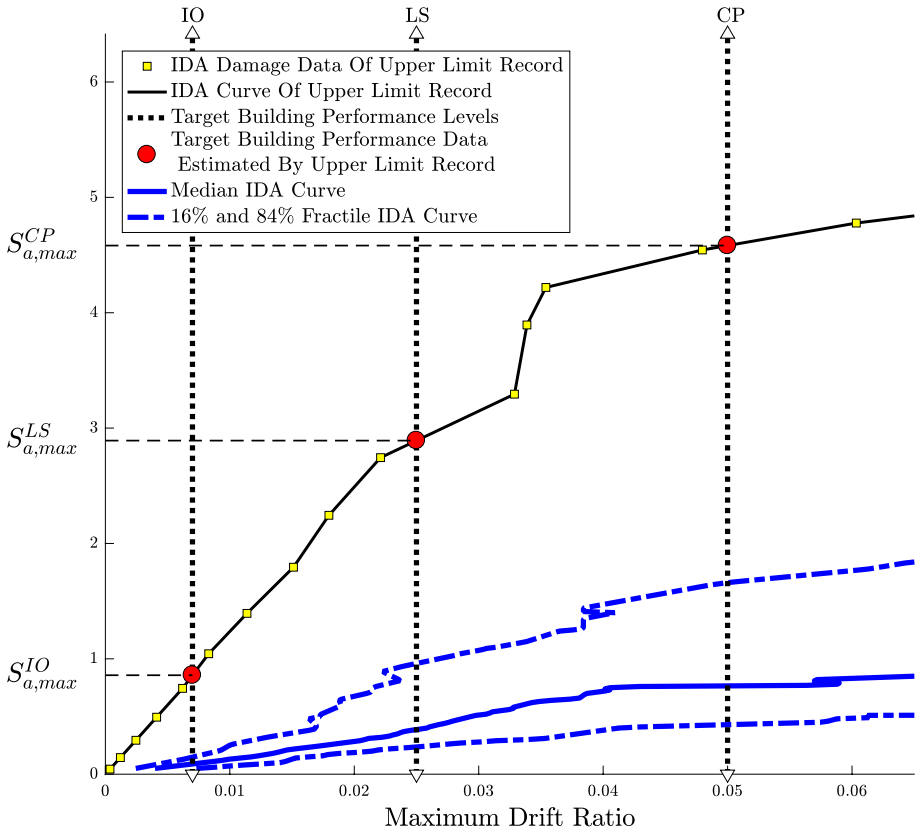

Fig. 3 The maximum IM $(=\mathrm{Sa}(T_1, \zeta))$ values correspond to three target building performance levels of IO, LS, and CP in the 8-story SMF frame obtained through IDA analyses by extreme record

is based on the interpretation of the potential hazard levels attained in a performance-based earthquake engineering framework. For example, for a given site, hazard curves corresponding to 2%, 5%, and 10% in 50 years, exceedance probability can be used.

6 State-based philosophy versus multi-strip analysis

The method used in this research has similarities and differences with multiple-strip analyzes (MSA). Three main differences between these methods are:

(1) Unlike MSA, which uses non-scaled records, all the analyzes used in the present study are of type IDA, in which records are scaled incrementally.
(2) In this study, only one set of ground motion records are selected to perform analysis in all IMs strips, while MSA uses a distinct record set in each analytical strip.
(3) In the present SBP fragility procedure, the selective IMs strips have not been extracted from hazard curves.

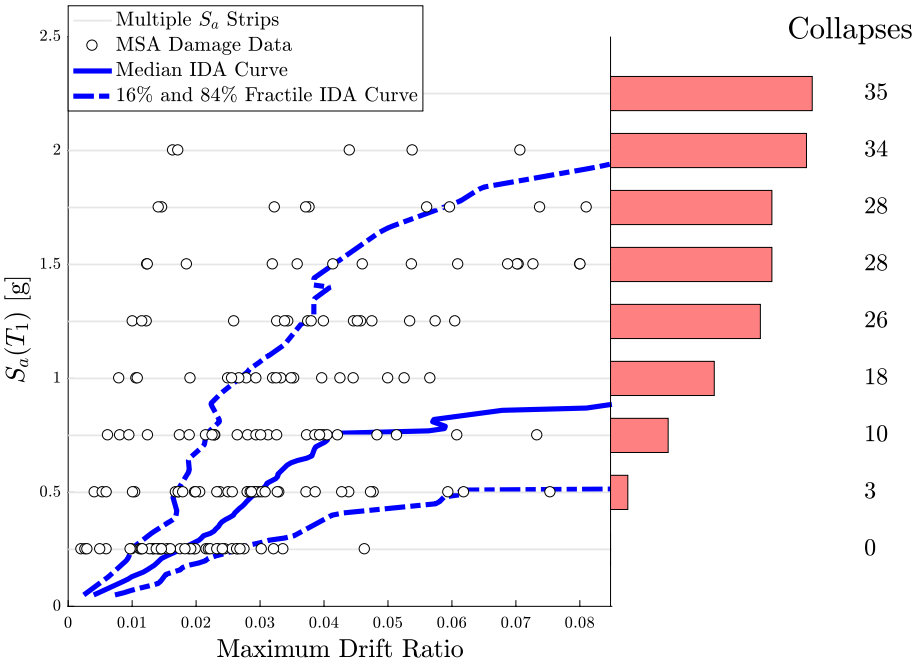

Fig. 4 An example of the IDA analysis results for an 8-story SMF structure

However, these two methods are similar in two ways:

(1) Both methods specify specific values for the IMs to perform time history analyses only on these values.
(2) The data obtained from MSA analysis is also used to obtain the fragility curve using the SBP method. Of course, in this research, MSA analysis was not directly used. However, if the number of strips used in MSA is equal to or more than the minimum required for the proposed method, the SBP fragility curve can also be fitted on results obtained from the multiple-strip analysis.

7 Fitting SBP fragility function on analytical data

In a determined structural model, after performing a series of nonlinear time-history analyses by using those ground motion records scaled at $IM = S_a^{Int}$, each record creates its own relative EDP value. Based on a comparison between these values and the EDP threshold of intended performance levels, it can be determined whether the exceeding occurs for a specific ground motion record or not. Next, by dividing the number of ground motion records reached the intended performance level threshold by the total number of ground motion records, a single point of the empirical cumulative distribution function (CDF) can be found (Eq. (11)).

$$P\left(\theta_{max} > \theta_{PL} | IM = S_a^{Int}\right) = n_{Ex}/N_{Total} \tag{11}$$

The sign of "*PL*" in Eq. (11) characterized the intended performance level. In this study, three separate performance level has been considered (*PL*=*IO* or *LS* or *CP*). So, by conducting an IDA analysis with several ground motion records scaled at $IM = \mathrm{S}_{\mathrm{a}}^{\mathrm{Int}}$, one can achieve two types of information: extreme record and one damage data point on CDF. As mentioned before, after establishing an extreme record, a complete IDA analysis should be performed by using this singular ground motion record to set the upper limits of intensity measure at each performance level (Sa_{max}^{IO},Sa_{max}^{LS}, and Sa_{max}^{CP}). Besides, performing a time-history analysis at $IM = \mathrm{S}_{\mathrm{a}}^{\mathrm{Int}}$ has another application similar to each IM strip's conventional usage in a multi-strips analysis procedure. Therefore, until this stage, two specific points on each intended performance level fragility curve is obtained. The first one is the point with $IM = S_a^{Int}$, which its collapse probability has been obtained from Eq. (11), and the second one with $IM = S_{a,max}^{PL}$.

To plot the fragility curve by the SBP method, some more auxiliary points must be generated. For this purpose, it is enough to conduct more analyses, just like what was done in $IM = S_a^{Int}$. That is to say, some other strip analyses in a various range of IM (=first mode spectral accelerations) must be done, and the values of the empirical cumulative distribution function (Eq. (11)) in each of them should be calculated consequently. Thus, one point of fragility curves related to each intended performance level will be achieved for each selected IM strip value.

If a series of IDA analyses are conducted using *m* number of IM strips and corresponding collapse EDPs for each ground motion record at these specified IM strips are recorded. The empirical CDF value for the intended performance level can be found on each strip (CDF_i^{PL}). Therefore, *m* different points on each empirical CDF associated with one performance level will be obtained. Next, three unknown parameters in the SBP fragility function (k_N, p, q) should be determined by fitting the SBP fragility function to obtained CDF damage data. This step is the most important one in the SBP method for finding the fragility curve since the SBP fragility function structure completely depends on these parameters. To achieve this goal, the values of IM strips must be normalized through Eq. (12).

$$\xi_i^{PL} = \frac{\left(S_a^{PL}\right)_i - S_{a,min}^{PL}}{S_{a,max}^{PL} - S_{a,min}^{PL}} \; i = 1, \ldots, m; PL = IO, LS, CP \tag{12}$$

By inserting the standardized dimensionless parameter ξ_i^{PL} in the SBP fragility function, a nonlinear system of will be forms as Eq. (13).

$$\begin{cases} FR_1^{PL}\left(\xi_1^{PL}; k_N, p, q\right) = CDF_1^{PL} \\ FR_i^{PL}\left(\xi_1^{PL}; k_N, p, q\right) = CDF_i^{PL} \\ FR_m^{PL}\left(\xi_m^{PL}; k_N, p, q\right) = CDF_m^{PL} \end{cases} \tag{13}$$

In Eq. (13) FR_i^{PL} represents the amount of SBP fragility function, introduced before in Eq. (8), at the ith point related to specific performance level *PL*. Despite the lack of an analytical solution for Eq. (13), a fitting method can solve it. For this purpose, firstly, Eq. (13) 's format should be changed into Eq. (14).

$$\begin{cases} f_1^{PL}\left(\xi_1^{PL}; k_N, p, q\right) = FR_1^{PL}\left(\xi_1^{PL}; k_N, p, q\right) - CDF_1^{PL} \\ f_m^{PL}\left(\xi_m^{PL}; k_N, p, q\right) = FR_m^{PL}\left(\xi_m^{PL}; k_N, p, q\right) - CDF_m^{PL} \end{cases} \tag{14}$$

In fact, Eq. (13) transforms to an optimization problem aimed to minimize function f^{PL} through nonlinear least square technique (Eq. (15)).

$$minf^{PL}\left(\xi^{PL};k_N,p,q\right)=min\sum_{i=1}^{m}\left(f_i^{PL}\left(\xi_i^{PL};k_N,p,q\right)\right)^2 \tag{15}$$

Some optimization algorithms, such as the Trust Region, can solve optimization problems more efficiently.

8 Selecting proper values for IM strips

An important issue to be addressed at this stage is the number of analytical strips and determining the intensity measure's values corresponding to each of them. On the one hand, the higher number of IM strips (m) used in the analysis process leads to more accurate fragility curves fitted with obtained damage data. On the other hand, this rise in accuracy can significantly increase the number of NTHA analyses. Thus, to find the best balance between accuracy and computational effort, an appropriate number of IM strips should be considered and employed.

For each SMF frame model used in this study, four categories of IM strips were considered. The number of strips used in each category differs as well as their IM values. The number of strips used in each of the intended categories is $m=5$, 7, 9, and 11, while for selecting IM strip values, one can easily select them in a step by step increase process. For example, when $m=5$ these strip values can be considered:$S_a^1=0.2g$, $S_a^2=0.4g$, $S_a^3=0.6g$, $S_a^4=0.8g$,$S_a^5=\mathrm{S_a^{Int}}$. Nevertheless, in some cases, such a choice will lessen the method's accuracy since this selection is made without considering the upper limits of different performance levels. For example, no IM strip may be chosen smaller than $\mathrm{S_{a,max}^{IO}}$ or all IM strips fall within the initial 20% IM range of the fragility curve for the *CP* performance level ($S_a^i<0.2S_{a,max}^{CP}$ for i = 1, … , m). To prevent such a problem and achieve the best accuracy for all the fragility curves corresponding to the different target performance

Table. 1 Selected IM strips values for four different categories

	5 Strips (m = 5)	7 Strips (m = 7)	9 Strips (m = 9)	11 Strips (m = 11)
S_a^1	$0.2\mathrm{S_{a,max}^{IO}}$	$0.1\mathrm{S_{a,max}^{IO}}$	$0.1\mathrm{S_{a,max}^{IO}}$	$0.1\mathrm{S_{a,max}^{IO}}$
S_a^2	$0.6\mathrm{S_{a,max}^{IO}}$	$0.4\mathrm{S_{a,max}^{IO}}$	$0.4\mathrm{S_{a,max}^{IO}}$	$0.4\mathrm{S_{a,max}^{IO}}$
S_a^3	$\mathrm{S_{a,max}^{IO}}+0.1\Delta S_a^{\mathrm{I}}$	$0.7\mathrm{S_{a,max}^{IO}}$	$0.7\mathrm{S_{a,max}^{IO}}$	$0.7\mathrm{S_{a,max}^{IO}}$
S_a^4	$\mathrm{S_{a,max}^{IO}}+0.4\Delta S_a^{\mathrm{I}}$	$\mathrm{S_{a,max}^{IO}}+0.1\Delta S_a^{\mathrm{I}}$	$\mathrm{S_{a,max}^{IO}}+0.1\Delta S_a^{\mathrm{I}}$	$\mathrm{S_{a,max}^{IO}}+0.1\Delta S_a^{\mathrm{I}}$
S_a^5	$\mathrm{S_a^{Int}}$	$\mathrm{S_{a,max}^{IO}}+0.4\Delta S_a^{\mathrm{I}}$	$\mathrm{S_{a,max}^{IO}}+0.4\Delta S_a^{\mathrm{I}}$	$\mathrm{S_{a,max}^{IO}}+0.4\Delta S_a^{\mathrm{I}}$
S_a^6	–	$\mathrm{S_{a,max}^{IO}}+0.7\Delta S_a^{\mathrm{I}}$	$\mathrm{S_{a,max}^{IO}}+0.7\Delta S_a^{\mathrm{I}}$	$\mathrm{S_{a,max}^{IO}}+0.7\Delta S_a^{\mathrm{I}}$
S_a^7	–	$\mathrm{S_a^{Int}}$	$\mathrm{S_{a,max}^{LS}}+0.1\Delta S_a^{\mathrm{II}}$	$\mathrm{S_{a,max}^{LS}}+0.1\Delta S_a^{\mathrm{II}}$
S_a^8	–	–	$\mathrm{S_{a,max}^{LS}}+0.4\Delta S_a^{\mathrm{II}}$	$\mathrm{S_{a,max}^{LS}}+0.4\Delta S_a^{\mathrm{II}}$
S_a^9	–	–	$\mathrm{S_a^{Int}}$	$\mathrm{S_{a,max}^{LS}}+0.7\Delta S_a^{\mathrm{II}}$
S_a^{10}	–	–	–	$\mathrm{S_{a,max}^{LS}}+0.9\Delta S_a^{\mathrm{II}}$
S_a^{11}	–	–	–	$\mathrm{S_a^{Int}}$

$\Delta S_{\mathrm{a}}^{\mathrm{I}}=\left(\mathrm{S_{a,max}^{LS}}-\mathrm{S_{a,max}^{IO}}\right)$ and $\Delta S_a^{\mathrm{II}}=\left(\mathrm{S_{a,max}^{LS}}-\mathrm{S_{a,max}^{IO}}\right)$

levels simultaneously, the selected IM strips should be scattered appropriately between the IM intervals of all the target performance levels.

If the goal is only to obtain a fragility curve for a single performance level, selecting the analytical tapes' values is simple. It can be done by a step by step algorithm as described above. However, if the goal is to obtain fragility curves at several performance levels simultaneously, certain complexities will be added to this selection process. One point to consider is that when an IM strip is selected for the middle range of the fragility curve related to a specific performance level, the same amount of IM for the higher performance level is likely to fall within the primary IM range. Therefore, as the intended performance level switch to the higher one, the requirement for selecting small IM strip amounts is lessened. In this study, the dispersion of the selected IM strip values is selected so that each fragility curve covers at least two numerical damage data points (in case that $m=5$ and $PL=IO$). These covered strips numbers can increase remarkably to 11 when the performance level switch to CP ($m=11$, PL = CP). When the number of strips used is lower, most strips should be selected in the range below $S_{a,max}^{LS}$ to ensure adequate accuracy for fragility curves of low-performance levels. However, this strip selection strategy can reduce the precisely fitted fragility curve at the end regions for higher performance levels. In this case, a suitable choice of S_a^{Int}, which is large enough, can be considered to compensate for this reduction in accuracy. Therefore, a reasonable procedure for selecting the IM strips' values can be considered as adding the upper limit of the lower yield level with a percentage of higher upper limit performance level as it is presented in Table. 1. In Table. 1, IM values related to each analytical strip are sorted from small to large in all columns. The only exception to this is the value of S_a^{Int}, which depends on the analyst's choice.

The results of IDA analyses for a 4-story SMF frame conducted with ground motions scaled at strips are shown in Table. 1 is presented in Fig. 5. Additionally, in this figure, the validity of *extreme record upper limits* assumption can be assessed visually. As can be seen maximum relative displacement for all records is less than the calculated value by this assumption.

9 State-based philosophy fragility curves

After obtaining the IDA analyses results (conducted using 44 ground motions scaled at specific intensity measures strips) the unknown parameters of the SBP fragility function can be obtained. This can be done by performing a fitting process on IDA results data. Ultimately, the parameters used in the SBP fragility function are derived through an optimization process introduced in Eq. 14 and 15. After specifying these parameters, the structure of the SBP fragility function is completed. In Figs. 6 and 7, the SBP fragility curves of four SMF models (2, 4, 8, and 12 stories frames) are plotted regarding three *IO*, *LS*, and *CP* target performance levels. Moreover, in these figures, the log-normal distribution function's fragility curves are plotted for better comparison.

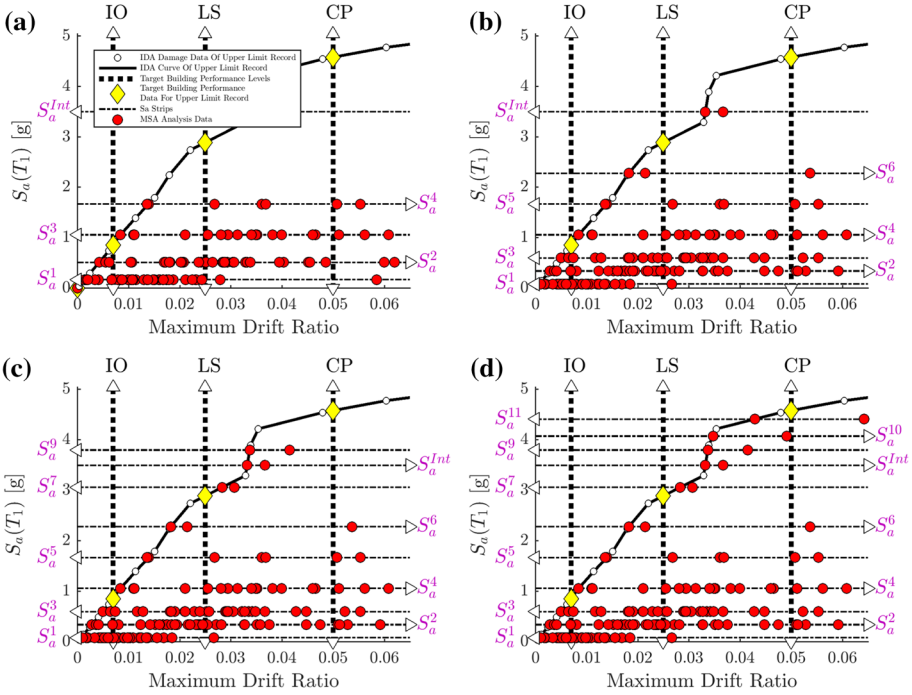

Fig. 5 Selecting IM strips for an 8 story SMF frame with **a** 5 strips **b** 7 strips **c** 9 strips **d** 11 strips

Comparing the SBP method with the usual log-normal method is shown in Tables 2, 3 and 4 in quantitative terms. Table 2 shows the information associated with the upper Limit Record. As can be seen from the 44 seismic records, only two records have generated maximum response values in the structure. These two records do not have an equal distribution in the different strip patterns, and three-quarters of the total maximum responses in all strip patterns were created by a single record (Chi-Chi, Taiwan-CHY101). The spectral acceleration at the fundamental period values considered in each of the strips is also specified in this table.

Table. 3 shows the results of optimizing the data obtained in each of the analytical strips to find the unknown parameters in the structure of the SBP fragility function corresponding to each of the triple performance levels. The Sa(T1,ζ) maximum values in different strips while the structure experiences vibration under the upper limit record are also mentioned in this table (S_{max}). For performance levels other than collapse, the

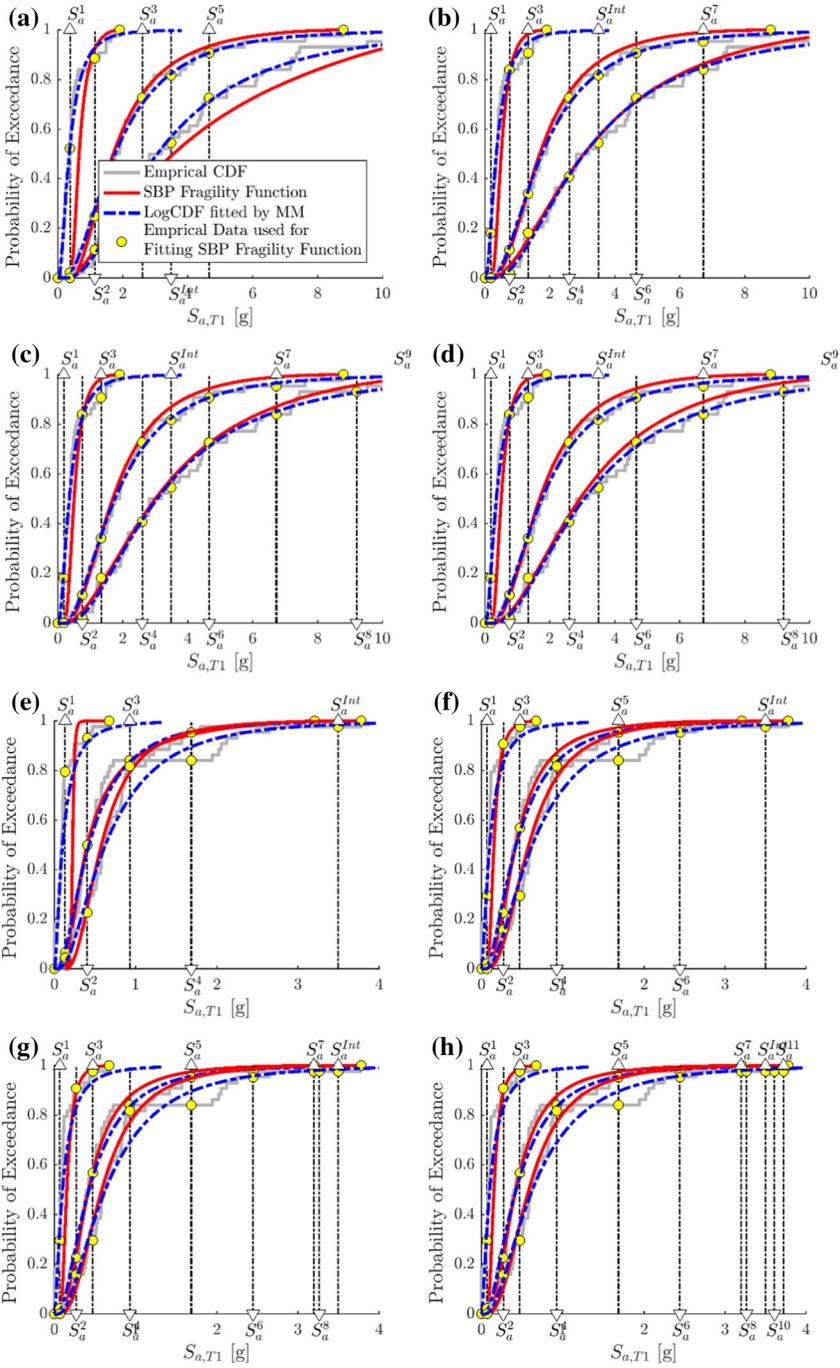
(a)
(b)
(c)
(d)
(e)
(f)
(g)
(h)
Probability of Exceedance
$S_{a,T1}$ [g]
Emprical CDF
SBP Fragility Function
LogCDF fitted by MM
Emprical Data used for Fitting SBP Fragility Function

◀ **Fig. 6** Log-normal and SBP fragility curves versus CDF values for four SMF frames **a** 2 story and 5 strips; **b** 2 story and 7 strips; **c** 2 story and 9 strips; **d** 2 story and 11 strips; **e** 4 story and 5 strips; **f** 4 story and 7 strips; **g** 4 story and 9 strips; **h** 4 story and 11 strips

number of data that can be used may not be exactly equal to the number of analytical strips. This relates to the selection strategy for determining the corresponding $S_a(T_1, \zeta)$ values for each analytical strip, mentioned in Table 1 earlier.

Table 4 answers how efficient the integration of data from analytical strips and SBP fragility function is and whether they can significantly reduce computational efforts without compromising the accuracy of the fragility curve. In this table, the degree of matching the results of the technique introduced in this study with the results of the data obtained from the complete IDA analyses are presented. To achieve a more comprehensive and accurate comparison, the effective parameters in the log-normal fragility function and the appropriateness of this function with complete IDA data are also given. Significant reductions in the number of computational efforts, especially if a smaller number of computational tapes are used, while maintaining accuracy in the fragility curve, confirm the new technique's effectiveness. Of course, as the number of analytical strips increases, the number of computations will also increase significantly. In Table 4, *the Average Error* and *Percent Reduction* columns can quantitatively demonstrate the strength of the SBP method for fragility analysis. The first column shows the amount of error obtained from plotting the fragility curve using the SBP method. The second one represents the percentage of reduction in nonlinear time history analysis resulting from the use of this method. It is necessary to mention that negative percentages in Table 4 are considered as an increase in the number of analyzes. From the results listed in Table 4, it is clear that fewer analytical strips have a far advantage over the high number of these strips.

10 Conclusion

The general format of the SBP fragility function (Eq. (8)) was obtained in previous studies. However, in this study, an innovative technique was introduced that is both fast and simple to determine each of the parameters present in this function. For this purpose, it is necessary to follow the steps below in order:

Step 1 Selecting a recordset to perform fragility analysis.

Step 2 Determining an appropriate IM value for the first strip ($S^{Int}_{a,T1}$). For SMF structures modeled in this study, a value between 1 and 2 g is recommended.

Step 3 Identifying extreme records by using a strip analysis at $S^{Int}_{a,T1}$. Extreme record causes the most dynamic response (here maximum drift ratio) in the structure.

Step 4 Performing a conventional IDA analysis by scaling the extreme record specified in step 3. The scaling process continues until the structural response exceeds the limit value of the highest desired performance level. At the end of this step, the maximum structural

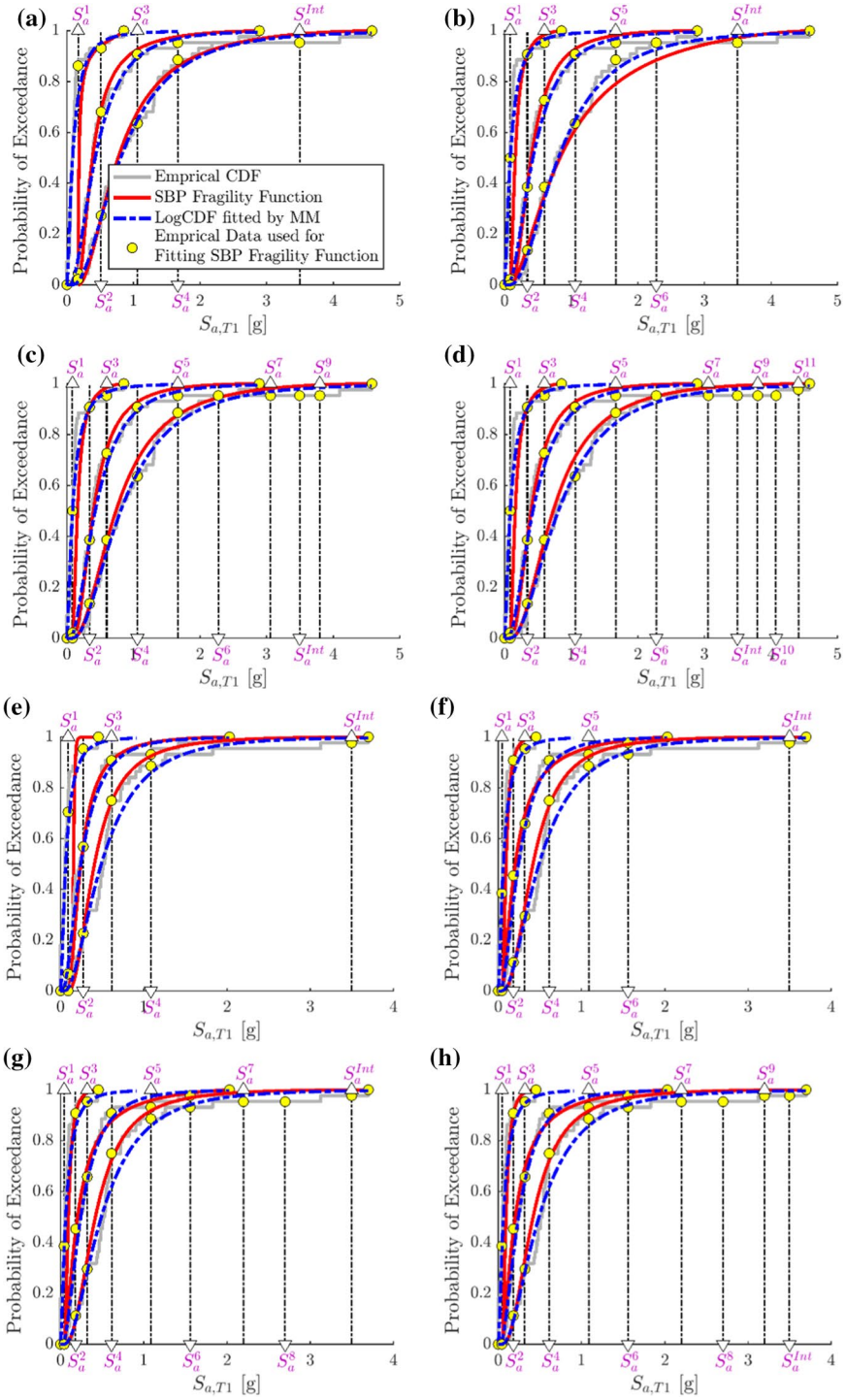
(a)
(b)
(c)
(d)
(e)
(f)
(g)
(h)
Probability of Exceedance
$S_{a,T1}$ [g]
Emprical CDF
SBP Fragility Function
LogCDF fitted by MM
Emprical Data used for Fitting SBP Fragility Function

◀ **Fig. 7** Log-normal and SBP fragility curves versus CDF for four SMF frames **a** 8 story and 5 strips; **b** 8 story and 7 strips; **c** 8 story and 9 strips; **d** 8 story and 11 strips; **e** 12 story and 5 strips; **f** 12 story and 7 strips; **g** 12 story and 9 strips; **h** 12 story and 11 strips

response values for each of the desired performance levels will be obtained (Fig. 3). These values are symbolized by $S_{a,max}^{PL}$ for each performance level (PL) and will be placed in Eq. (12) to standardize the input data for the SBP fragility function (ξ_i^{PL}).

Step 5 At this stage, some strip analyzes must be performed at different IMs. Then, the value of the experimental cumulative distribution function in each strip can be calculated, and consequently, one point of the empirical fragility curve will be achieved. To increase the precision of the fragility curve in all structural behavior regions, the values in Table 1 are recommended for IM strip values.

Step 6 In this step, by fitting the SBP fragility function to the points obtained in the fifth step, the unknown parameters in the SBP fragility function (k_N, p, q) are extracted (Eqs. (14) and (15)).

After following the steps described above, the final products are SBP fragility curves, as shown in Figs. 6 and 7. In order to compare, a different number of analytical strips were used in the present study. Finally, the results indicated that increasing these strips, although significantly increasing the number of analyses, had little effect on the results' accuracy. It was observed that the analysis reduced the number of analyzes by 50% by using only five analytical strips while providing very high accuracy. This means that the fragility curve based on only one or two middle strips can be substituted with the usual method's fragility curve with appropriate accuracy. After observing and comparing the results obtained in this study, the SBP-based fragility function's strength was approved again. In fact, this function has a unique ability to provide the fragility curve practically and accurately while requiring less time history analysis than usual.

Table. 2 Determination of the extreme record and information obtained from structural analysis with this record

	S_a^{Int}[g]	Upper limit record earthquake station	Sa Strips [g]
SBP-5 Strips			
2 St	3.5	Chi-Chi, Taiwan-CHY101	0.3822,1.1466,2.5997,3.5,4.666
4 St	3.5	Chi-Chi, Taiwan-CHY101	0.13556,0.40669,0.93075,1.6895,3.5
8 St	3.5	Kocaeli, Turkey-Duzce	0.17157,0.51471,1.0612,1.6714,3.5
12 St	3.5	Chi-Chi, Taiwan-CHY101	0.091649,0.27495,0.61592,1.0889,3.5
SBP-7 Strips			
2 St	3.5	Chi-Chi, Taiwan-CHY101	0.1911,0.76439,1.3377,2.5997,3.5,4.666,6.7323
4 St	3.5	Chi-Chi, Taiwan-CHY101	0.067782,0.27113,0.47447,0.93075,1.6895,2.4483,3.5
8 St	3.5	Kocaeli, Turkey-Duzce	0.085786,0.34314,0.6005,1.0612,1.6714,2.2815,3.5
12 St	3.5	Chi-Chi, Taiwan-CHY101	0.045825,0.1833,0.32077,0.61592,1.0889,1.562,3.5
SBP-9 Strips			
2 St	3.5	Chi-Chi, Taiwan-CHY101	0.1911,0.76439,1.3377,2.5997,3.5,4.666,6.7323,9.2071,10.4324
4 St	3.5	Chi-Chi, Taiwan-CHY101	0.067782,0.27113,0.47447,0.93075,1.6895,2.4483,3.2,3.2644,3.5
8 St	3.5	Kocaeli, Turkey-Duzce	0.085786,0.34314,0.6005,1.0612,1.6714,2.2815,3.0607,3.5,3.8
12 St	3.5	Chi-Chi, Taiwan-CHY101	0.045825,0.1833,0.32077,0.61592,1.0889,1.562,2.2016,2.7015,3.5
SBP-11 Strips			
2 St	3.5	Chi-Chi, Taiwan-CHY101	0.1911,0.76439,1.3377,2.5997,3.5,4.666,6.7323,9.2071,10.4324,11.6578,12.4747
4 St	3.5	Chi-Chi, Taiwan-CHY101	0.067782,0.27113,0.47447,0.93075,1.6895,2.4483,3.2,3.2644,3.5,3.6087,3.7234
8 St	3.5	Kocaeli, Turkey-Duzce	0.085786,0.34314,0.6005,1.0612,1.6714,2.2815,3.0607,3.5,3.8,4.075,4.4132
12 St	3.5	Chi-Chi, Taiwan-CHY101	0.0458,0.1833, 0.3208,0.6159,1.0889, 1.5620,2.2016,2.7015, 3.2013,3.5000

Table. 3 Parameters of SBP fragility function derived from the process of optimizing the data obtained from the analytical strips

	IO					LS					CP				
	kN	p	Q	S_{max}	N.E.D	kN	p	Q	S_{max}	N.E.D	kN	p	Q	S_{max}	N.E.D
5 Strips SBP Fragility Function															
2 St	3.494	1.046	0.001	1.911	3	3.695	0.970	0.359	8.799	5	1.807	0.701	2.254	12.883	5
4 St	91.369	3.534	4.512	0.678	3	4.102	0.732	1.006	3.207	5	6.024	1.118	0.000	3.781	5
8 St	4.034	0.409	0.001	0.858	3	5.770	0.861	0.012	2.892	5	3.991	0.924	0.500	4.582	5
12 St	88.780	3.715	4.389	0.458	3	6.391	0.912	0.000	2.035	5	7.856	1.067	0.000	3.701	5
7 Strips SBP Fragility Function															
2 St	4.118	1.186	0.000	1.911	4	3.845	1.083	0.282	8.799	7	2.412	0.903	0.746	12.883	7
4 St	5.266	1.155	0.458	0.678	4	5.780	1.046	0.177	3.207	7	5.458	1.151	0.006	3.781	7
8 St	5.030	0.888	0.015	0.858	4	6.075	1.067	0.000	2.892	7	2.858	0.812	2.485	4.582	7
12 St	5.441	1.057	0.000	0.458	4	4.556	0.749	0.442	2.035	7	7.980	1.163	0.000	3.701	7
9 Strips SBP Fragility Function															
2 St	4.118	1.186	0.000	1.911	4	3.845	1.083	0.282	8.799	8	2.501	0.925	0.605	12.883	9
4 St	5.266	1.155	0.458	0.678	4	5.998	1.065	0.023	3.207	8	5.429	1.149	0.063	3.781	9
8 St	5.030	0.888	0.015	0.858	4	6.075	1.067	0.000	2.892	7	4.333	1.024	0.336	4.582	9
12 St	5.441	1.057	0.000	0.458	4	4.556	0.749	0.442	2.035	7	7.555	1.134	0.000	3.701	9
11 Strips SBP Fragility Function															
2 St	4.118	1.186	0.000	1.911	4	3.845	1.083	0.282	8.799	8	2.731	0.984	0.364	12.883	11
4 St	5.266	1.155	0.458	0.678	4	5.998	1.065	0.023	3.207	8	5.436	1.149	0.061	3.781	11
8 St	5.030	0.888	0.015	0.858	4	6.075	1.067	0.000	2.892	7	4.592	1.056	0.131	4.582	11
12 St	5.441	1.057	0.000	0.458	4	4.556	0.749	0.442	2.035	7	7.521	1.132	0.000	3.701	11

NED Number of empirical data used to extract fragility function parameters

Table. 4 The degree of conformity of the results of the new SBP technique with the results of the complete IDA analysis and the rate of reduction of the calculations due to the use of this technique

	IO	LS	CP	N.A	Avg. Err	P.R	IO	LS	CP	N.A	Avg. Err	P.R
	5 Strips SBP Fragility Function						7 Strips SBP Fragility Function					
2 St	90%	97%	90%	257	7.67%	80%	89%	98%	92%	345	7%	73%
4 St	79%	93%	95%	237	11%	50%	93%	97%	96%	325	4.67%	31%
8 St	78%	90%	98%	237	11.33%	57%	95%	97%	94%	325	4.67%	41%
12 St	79%	96%	94%	237	10.33%	47%	96%	96%	95%	325	4.33%	27%
	9 Strips SBP Fragility Function						11 Strips SBP Fragility Function					
2 St	89%	98%	93%	433	6.67%	66%	89%	98%	93%	521	6.67%	59%
4 St	93%	97%	96%	413	4.67%	12%	93%	97%	96%	501	4.46%	-6%
8 St	95%	97%	97%	413	3.67%	25%	95%	97%	97%	501	3.67%	9%
12 St	96%	96%	95%	413	4.33%	7%	96%	96%	95%	457	4.33%	-2%
	Log-normal CDF Based on IDA Analysis Data											
	IO Mean	IO SD	LS Mean	LS SD	CP Mean	CP SD	IO	LS	CP	N.A	Avg. Err	
2 St	0.356	0.798	1.760	0.734	3.061	0.755	97%	98%	98%	1285	2.33%	
4 St	0.103	1.006	0.428	0.796	0.630	0.782	91%	96%	96%	471	5.67%	
8 St	0.088	1.050	0.427	0.728	0.809	0.710	94%	96%	98%	550	4%	
12 St	0.065	0.992	0.245	0.763	0.492	0.739	92%	96%	96%	446	5.33%	

NA Number of Analyses; *PR* Percent Reduction; *Avg. Err* Average Error

Declarations

Conflicts of interest No funds, grants, or other support was received.

References

ATC (2009) Quantification of building seismic performance factors

Baharvand A, Ranjbaran A (2020a) A New method for developing seismic collapse fragility curves grounded on state-based philosophy. Int J Steel Struct. https://doi.org/10.1007/s13296-020-00308-6

Baharvand A, Ranjbaran A (2020b) Seismic fragility functions grounded on state-based philosophy: application to low to midrise steel frame buildings. KSCE J Civ Eng. https://doi.org/10.1007/s12205-020-0350-5

Bakalis K, Vamvatsikos D (2018) Seismic fragility functions via nonlinear response history analysis. J Struct Eng 144:04018181. https://doi.org/10.1061/(ASCE)ST.1943-541X.0002141

Baker JW (2015) Code supplement to efficient analytical fragility function fitting using dynamic structural analysis. Earthq Eng Res Inst 31:579–599. https://doi.org/10.1193/021113EQS025M

Casotto C, Silva V, Crowley H et al (2015) Seismic fragility of Italian RC precast industrial structures. Eng Struct 94:122–136. https://doi.org/10.1016/j.engstruct.2015.02.034

Cremen G, Baker JW (2018) Quantifying the benefits of building instruments to FEMA P-58 rapid post-earthquake damage and loss predictions. Eng Struct 176:243–253. https://doi.org/10.1016/j.engstruct.2018.08.017

Elkady A, Lignos DG (2014) Modeling of the composite action in fully restrained beam-to-column connections: implications in the seismic design and collapse capacity of steel special moment frames. Earthquake Eng Struct Dynam 43:1935–1954. https://doi.org/10.1002/eqe.2430

FEMA P (2009) Quantification of Building Seismic Performance Factors (FEMA P695, ATC-63)

Hartloper A, Lignos D (2017) 11.29: Updates to the ASCE-41–13 provisions for the nonlinear modeling of steel wide-flange columns for performance-based earthquake engineering. Ce/Papers 1:3072–3081. https://doi.org/10.1002/cepa.359

Hasik V, Chhabra JPS, Warn GP, Bilec MM (2018) Review of approaches for integrating loss estimation and life cycle assessment to assess impacts of seismic building damage and repair. Eng Struct 175:123–137. https://doi.org/10.1016/j.engstruct.2018.08.011

Jalayer F (2003) Direct probabilistic seismic anaysis: implementing nonlinear dynamic assessments. Stanford University, Stanford

Jalayer F, Elefante L, De RR, Manfredi G (2014) Cloud analysis revisited : efficient fragility calculation and uncertainty propagation using simple linear regression. Tenth US Natl Conf Earthq Eng. https://doi.org/10.4231/D3SF2MC59

Kappos AJ (2016) An overview of the development of the hybrid method for seismic vulnerability assessment of buildings. Struct Infrastruct Eng 12:1573–1584. https://doi.org/10.1080/15732479.2016.1151448

Lignos DG, Krawinkler H (2011) Deterioration modeling of steel components in support of collapse prediction of steel moment frames under earthquake loading. J Struct Eng 137:1291–1302. https://doi.org/10.1061/(ASCE)ST.1943-541X.0000376

Mazzoni S, McKenna F, Scott MH, Fenves GL (2006) The open system for earthquake engineering simulation (OpenSEES) user command-language manual

Michel C, Crowley H, Hannewald P et al (2018) Deriving fragility functions from bilinearized capacity curves for earthquake scenario modelling using the conditional spectrum. Bull Earthq Eng 16:4639–4660. https://doi.org/10.1007/s10518-018-0371-3

Noh HY, Lallemant D, Kiremidjian AS (2015) Development of empirical and analytical fragility functions using kernel smoothing methods. Earthquake Eng Struct Dynam 44:1163–1180

Padgett JE, DesRoches R (2008) Methodology for the development of analytical fragility curves for retrofitted bridges. Earthq Eng Struct Dyn. https://doi.org/10.1002/eqe

Ranjbaran A, Ranjbaran M (2016) State functions: the milestone of fracture. Arch Appl Mech 86:1311–1324. https://doi.org/10.1007/s00419-015-1115-3

Shafei B, Zareian F, Lignos DG (2011) A simplified method for collapse capacity assessment of moment-resisting frame and shear wall structural systems. Eng Struct 33:1107–1116. https://doi.org/10.1016/j.engstruct.2010.12.028

Shome N, Cornell C (1999) Probabilistic seismic demand analysis of nonlinear structures. Stanford University, Stanford

Tekie PB, Ellingwood BR (2003) Seismic fragility assessment of concrete gravity dams. Earthq Eng Struct Dyn 32:2221–2240. https://doi.org/10.1002/eqe.325

Vamvatsikos D, Cornell CA (2002) Incremental dynamic analysis. Earthquake Eng Struct Dynam 31:491–514. https://doi.org/10.1002/eqe.141

Vamvatsikos D, Cornell CA (2004) Applied incremental dynamic analysis. Earthq Spectra 20:523–553. https://doi.org/10.1193/1.1737737

Vamvatsikos D, Cornell CA (2005) Developing efficient scalar and vector intensity measures for IDA capacity estimation by incorporating elastic spectral shape information. Earthquake Eng Struct Dynam 34:1573–1600. https://doi.org/10.1002/eqe.496

Vargas YF, Pujades LG, Barbat AH, Hurtado JE (2013) Capacity, fragility and damage in reinforced concrete buildings: A probabilistic approach. Bull Earthq Eng 11:2007–2032. https://doi.org/10.1007/s10518-013-9468-x

Xin D, Daniell JE, Wenzel F (2018) State of the art of fragility analysis for major building types in China with implications for intensity-PGA relationships. Nat Hazards Earth Syst Sci Discuss 1–34

Yun S, Hamburger RO, Cornell C, Foutch DA (2002) Seismic performance evaluation for steel moment frames. J of Struct Eng, ASCE 128:534–545. https://doi.org/10.1061/(ASCE)0733-9445(2002)128:4(534)

Zareian F, Krawinkler H, Ibarra L, Lignos D (2010) Basic concepts and performance measures in prediction of collapse of buildings under earthquake ground motions. Struct Des Tall Spec Build. Struct Design Tall Spec Build 16:167–181. https://doi.org/10.1002/tal.546